A Systematic Study on Notched Impact Strength of Super-Toughened Polyamide 6 Nanocomposites Using Response Surface Methodology

Hadi Ramezani-Dakhel, Hamid Garmabi

Department of Polymer Engineering and Color Technology, Amirkabir University of Technology, Tehran, Iran

Received 10 November 2009; accepted 14 March 2010
DOI 10.1002/app.32458
Published online 27 May 2010 in Wiley InterScience (www.interscience.wiley.com).

ABSTRACT: Response surface methodology was utilized to optimize the impact strength of polyamide 6 based nanocomposites using three different types of tougheners (ethylene-methyl acrylate, ethylene-ethyl acrylate-maleic anhydride, and hydrogenated butadiene acrylonitrile rubber) at three different levels of clay and rubber. Melt mixing method using a lab scale twin screw extruder was applied to prepare the samples. The wide-angle X-ray diffraction, transmission electron microscopy, and atomic force microscopy results indicated intercalated/exfoliated morphology for all of the prepared nanocomposites. The tensile properties as well as the Izod impact strength of the designed samples were evaluated. Impact resistance was correlated to material variables by using a second order polynomial function. The best balanced mechanical properties, between 15 designed experiments, was achieved using ethylene-ethyl acrylate-maleic anhydride as toughener, 4 wt % of clay and 17.5 wt % of the toughener, whereas 900% improvement in impact strength and 15% enhancement of Young's modulus was obtained compared with pristine polyamide 6 resin. The formulation meeting the simultaneous optimization of Young's modulus and impact strength was proposed based on mathematical quadratic modeling. © 2010 Wiley Periodicals, Inc. J Appl Polym Sci 118: 969–979, 2010

Key words: hybrid nanocomposites; nylon 6; impact resistance

INTRODUCTION

Polymer-layered silicate nanocomposites challenge traditional filled polymers in many industrial applications by presenting similar physical improvements using much lower nanofiller concentrations. Previous reports on polymer-layered silicate nanocomposites indicate increased modulus,[1–3] impact strength,[1,2,4,5] heat distortion temperature[6–8] and barrier properties[9–12] with decreased thermal expansion coefficient[13] compared with their pristine polymers.

Nylon-6 nanocomposites have been the most extensively studied semicrystalline nanocomposite to date. These nanocomposites exemplify a significant improvement of all properties by means of platelet-like nanoclay. The only limitation of these systems is their low fracture toughness.

Many scientists have shown that the impact performance of semicrystalline polymers as same as polyamides can be significantly enhanced by inclusion of rubber particles.[14–17] A salient toughening effect is achieved when the rubber phase forms a submicron-sized dispersion. However, this toughening technique often entails an extensive rubber content (5–25 wt %) which, in turn, involves a considerable decrease in elastic modulus. A question arises whether it is possible to achieve a substantial toughening without reduction of modulus with the help of both mineral platelet particles and rubber. If such were the case, it should then be promising to achieve tough materials exhibiting high impact strength as well as high modulus. Therefore, balancing between the clay content and the rubber content as well as choosing appropriate filler and rubber type incorporate with correct processing condition would be an acceptable route to achieve a high impact resistance compound with appropriate modulus.

So far, the majority of researches and developments have been focused on improving the impact resistance of polyamide based nanocomposites, while keeping the Young's modulus within an acceptable range. Cho et al.[18] prepared Nylon 6/organoclay nanocomposites through direct melt compounding by means of a conventional twin screw extruder. They illustrated that the mechanical properties of the organoclay nanocomposites were significantly increased with slight decrease in ductility. Kelnar et al.[19] studied the effect of clay treatment on mechanical behavior and nanostructure of polyamide

Correspondence to: H. Garmabi (garmabi@aut.ac.ir).
Contract grant sponsor: Iran National Science Foundation.

6/ethylene-propylene rubber (EPR) blends. They indicated that the insertion of clay with less polar treatment in the interfacial area gets an important new effect consisting intensification of toughening effect of dispersed elastomer by construction of "core-shell" particles. They stated that the rationalization of this effect, which almost certainly enhances the energy absorbing capacity of the plastically deformed zone around rubber particles (or may even support rubber cavitation), needs supplementary studies. Dasari et al.[20] examined the effect of blending sequence on microstructure of ternary nylon 66/clay/rubber (styrene-ethylene/butylene-styrene grafted with maleic andydride) nanocomposites. They concluded that blending nylon 66 and organoclay initially, and then mixing with rubber is the number one blending sequence to maximize the notched impact strength because locating of the organoclay in the rubber phase diminishes the latter's ability to cavitate, leading to reduced toughening effectiveness. Ahn et al.[21] prepared different formulations varying in montmorillonite, and maleated ethylene-propylene rubber content by mixing of nylon 6 and organoclay in a twin screw extruder and subsequently compounding the nanocomposites with the rubber in a single screw extruder. They illustrated that there is a clear swap between stiffness/strength versus toughness/ductility. As the clay content increase, the extent of plastic deformation reduces, which results into lower impact resistant of the obtained nanocomposite.

Recently, response surface method has been used successfully for material and process optimization in several studies.[22–26] This approach has the advantage of reducing the total number of required experiments while taking into consideration the mutual effects of several parameters. Response surface method uses statistical techniques to fit an empirical model to the experimental data. The use of a model to evaluate the effect of various parameters on impact resistance of polyamide based nanocomposites allows to characterize the affecting parameters in a straightforward and methodical way and to prognosticate the results of the experiments. Therefore, response surface method facilitates obtaining an overview of the influential parameters and their influence on each other. Furthermore, the surface contours of factors draw the processing window and point out the direction to get the optimum condition. This method is briefly enlightened in the next section.

Response surface methodology

In statistics, response surface methodology or RSM is a collection of mathematical and statistical procedures helpful for modeling and analysis of problems in which a response of interest is influenced by several variables and the purpose is to optimize the response. Response surface methodology explores the relationships between several explanatory variables and one or more response variables. The main thought of RSM is to employ a set of designed experiments to obtain an optimal response. The steps in the procedure are described briefly as follows. The parameters (ξ_1,ξ_2,ξ_3.....) affecting the response (η) should be chosen.The corresponding coded variables (x_1, x_2, x_3...) should be calculated by means of the following equation:

$$x_i = \frac{\xi_i - [\xi_{Ai} + \xi_{Bi}]/2}{[\xi_{Ai} - \xi_{Bi}]/2} \quad (1)$$

where ξ_{Ai} and ξ_{Bi} refer to the high and low levels of the variables ξ_i, respectively.

The empirical model by multiple regression analysis should be determined to produce theoretical responses ($\hat{y}$). The second-order model is extensively utilized in response surface methodology. The universal equation for response η of the second-order model is given by:

$$\eta = \beta_0 + \sum_{i=1}^{k} \beta_i x_i + \sum_{i=1}^{k} \beta_{ii} x_i^2 + \sum \sum_{i<j=2}^{k} \beta_{ij} x_i x_j + \varepsilon \quad (2)$$

where β_{ii} is the curvature term of independent variable and β_{ij} is the interaction coefficient between variables x_i and x_j. k is the number of factors and x_i are the coded variables. ε represents the random error in η. Assumptions made about this term are:

1. Zero mean and common variance, σ^2.
2. Mutually independent in the statistical sense.
3. Normally distributed.

Finally, the regression coefficients (β) to fit the experimental data as close as possible should be calculated. The correlation between the response and the variables is visualized by a response surface or contour plot to see the comparative influence of the parameters, to get an optimum parameter combination, and to predict the experimental results for other parameter combinations.

Box Behnken designs are fractional 3^k factorials. The designs either meet, or approximately meet, the criterion of rotatability. These designs are created by combination of two-level factorial designs with incomplete block designs. This procedure has been used in this study.

In this study, response surface method of experimental design was used to optimize the material parameters in twin-screw compounding of polyamide 6/rubber/nanoclay hybrid nanocomposites. The

rubber type, clay content, and rubber content are the three variables identified in this study. The objective was to use this empirical model to guide the future experiments and to produce high impact resistance compounds for future applications.

EXPERIMENTAL

Materials

Polyamide 6 (PA6) used in this study was Ultramid B5 (M_n = 42,000) obtained from BASF. Three different toughers were used to improve the impact toughness of the PA6 resin. The ethylene-methyl acrylate copolymer (EMA), Lotryl 29MA03, and ethylene-ethyl acrylate-maleic anhydride terpolymer (E-EA-MAH), Lotader 4700, both were kindly provided by Arkema and a fully hydrogenated butadiene acrylonitrile copolymer (HNBR), Therban A 3907, with less than 1% residual double bonds were obtained from Bayer Co. The nanofiller was Closite® 30B obtained from Southern Clay Products is organically modified montmorillonite with a quaternary ammonium salt. The as-received clay (montmorillonite) particles were disk-like stacks of silicate layers, 1 nm thick and varying in diameter from 100 nm to several microns. The specific gravity of the clay particles (stacks) is 1.98 and the layer spacing (d-spacing) is 1.84 mm. The modulus of an individual layer (platelet or flake) is 170–180 GPa and its specific gravity is 2.5.[27]

Preparation of nanocomposites

Formulations design in accordance with the response surface method is shown in Table I. As it can be seen, in the column of rubber type, −1, 0, and 1 stand for HNBR, Lotader 4700 and Lotryl 29MA03, respectively. All the materials were dried at 90°C overnight before processing. To achieve the highly intercalated/exfoliated structure, a two steps process (masterbatch approach) was utilized. At the first step, nanoclay and polyamide (16 wt % of nanoclay) were extruded and then, at the second stage, the required weight of polyamide, rubber, and masterbatch was melt blended to achieve the desired formulations. A lab scale Brabender corotating twin screw extruder, DSE25, (L/D = 40) was used for the compounding operations. The temperature of the extruder was set at 240, 245, 245, 240, and 245°C from hopper to die, respectively. The screw speed was maintained at 200 rpm. The product was granulated, dried, and injection molded using an 80 Ton injection molding machine at melt temperature of 250°C and mold temperature of 80°C.

TABLE I
Formulations According to the Response Surface Method of Experimental Design

No	Rubber type	Rubber type	Clay (%)	Rubber (%)
1	HNBR	−1	4	12.5
2	Lotader 4700	0	2	22.5
3	Lotader 4700	0	6	12.5
4	Lotryl 29MA03	1	4	12.5
5	Lotader 4700	0	6	22.5
6	HNBR	−1	6	17.5
7	Lotryl 29MA03	1	4	22.5
8	HNBR	−1	4	22.5
9	Lotader 4700	0	4	17.5
10	Lotader 4700	0	4	17.5
11	Lotader 4700	0	2	12.5
12	HNBR	−1	2	17.5
13	Lotader 4700	0	4	17.5
14	Lotryl 29MA03	1	2	17.5
15	Lotryl 29MA03	1	6	17.5

Testing

Both dog-bone tensile bars and notched Izod bars, kept in a desiccator for at least 88 h at ambient temperature. Therefore, the reported mechanical results would be at dry condition. Tensile tests were carried out using a Galdabini Su 2500 apparatus at a crosshead speed of 50 mm/min. The stress-at-break, elongation at break, fracture energy, and Young's modulus were evaluated as well. Izod impact tests were carried out on notched specimens using a Ueshima Seisakusho U-F impact tester. The notches (depth = 2.5±0.12 mm) were machined on the injection moulded samples.

Morphological observations

The surfaces of the cryogenically fractured specimens were observed using a Philips XL30 scanning electron microscope (SEM) after sputter gold coating. The Lotader and Lotryl containing samples were etched using boiling Xylene for 15 min and samples including HNBR stained using *n*-heptane for 3 h. Before commencement of final observations, the efficiency of etching process was confirmed by some preliminary observations. Wide-angle X-ray diffraction (XRD) patterns for the prepared compounds were recorded on a Phillips X'Pert diffractometer using CuKaα radiation (λ = 1.54056 nm). The diffractometer operated at a voltage of 40 kV and a current of 40 mA. The XRD data were collected from 1 to 10° (2Θ) with a scanning rate of 1.2 °/min. For transmission electron microscopy (TEM) observations, ultrathin sections were cut, under liquid N_2, from a stained (OsO_4 vapor for 24 h) sample to enhance the phase contrast among nylon 6, organoclay, and rubber phases using a Reichert OMU3 ultramicrotome. TEM studies were performed using

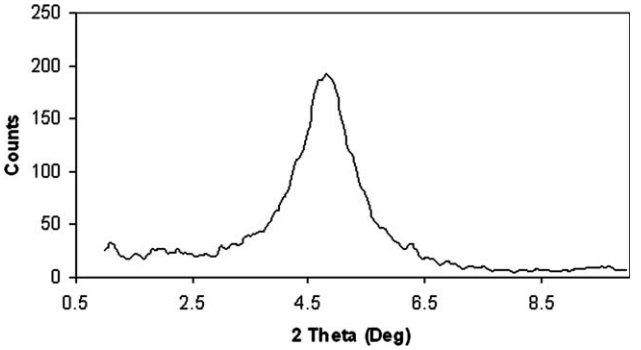

Figure 1 X-ray diffraction pattern of organoclay (Cloisite® 30B) showing the intra-gallery of organoclay (1.84 nm).

a Zeiss CEM902A operating at 80 kV. AFM observations were carried out on a Dualscope/Rasterscope C26 model supplied by Danish Micro Engineering A/S (DME). Both height (topography) and phase images were obtained in AC mode simultaneously. A probe with conical tip (with 15–20 micron height, the angle less than 20° and curvature radius less than 10 nm) at frequency of 150–190 kHz was employed.

RESULTS AND DISCUSSION

Characterization of the nanostructure

The characterization of the nanostructure of the hybrid systems was carried out using XRD, TEM, and AFM. The XRD plot of the Closite® 30B is shown in Figure 1. The organomontmorillonite shows the usual peaks at $2\Theta = 4.78^\circ$, which keeps up a correspondence to a basal spacing of 1.84 nm. The results of X-ray diffraction of the injection molded compounds are shown in Table II. A shift in the clay peak or disappearance of that peak indicates the formation of an intercalated or intercalated/exfoliated structure in all of the nanocomposites. As known, XRD is not a reliable tool for analyzing the complex dispersion of clay layers in ternary nanocomposites, particularly, polymer-rubber-clay systems, where the location of clay determines the exfoliation or intercalation phenomenon. Therefore, the transmission electron microscopy (TEM) technique was also employed to the nanostructure of the samples. The TEM micrograph of the sample No. 5 is shown in Figure 2(b). It was observed that the clay particles were partly exfoliated into single nanolayers randomly distributed in the matrix and partly intercalated in the form of randomly dispersed clusters of nanolayers confirming the results obtained from the X-ray diffraction. Also, the TEM micrograph of the sample No. 2 is shown in Figure 2(a) demonstrating well exfoliated silicate layers in the nylon-6 matrix. However, TEM includes a local observation and these micrographs do not confirm the same morphology throughout the sample.

AFM was also used to view the nanostructure of the samples, directly. This technique has been applied to probe the nanostructure of nanocomposites by some researchers.[9,28,29] AFM is a nondestructive test and sample preparation is not required unlike SEM and TEM techniques. AFM results (height and phase images) should be interpreted with some caution. Any changes in phase images (observing darker or lighter areas) would not simply imply the alteration in the nature of the substance (all dark areas could not be merely the inorganic (harder) substance). In fact, variation in the height of the surface can also result in observation of some

TABLE II
Izod Impact strength, Tensile Properties and X-Ray Diffraction Peaks of the Prepared Compounds

No	Izod impact strength (kJ/m^2)	E (MPa)	σ_{UTS} (MPa)	σ_y (MPa)	ε(%)	Fracture energy (J)	Particle size (nm)	2θ
1	9.5 ± 1.7	3378 ± 131	65 ± 3	65 ± 3	56 ± 9	56 ± 9	245 ± 10	2.1
2	99.1 ± 14.2	2151 ± 367	48 ± 3	46 ± 1	75 ± 9	63 ± 11	60 ± 2	–
3	14.2 ± 4.1	3827 ± 388	68 ± 5	68 ± 5	50 ± 6	56 ± 8	58 ± 3	1.9
4	8.0 ± 2.1	3287 ± 317	66 ± 3	66 ± 3	12 ± 2	11 ± 2	503 ± 27	1.9
5	13.7 ± 2.6	2029 ± 149	41 ± 2	–	10 ± 1	6 ± 1	86 ± 4	2.4
6	7.4 ± 1.2	4224 ± 195	70 ± 1	70 ± 1	36 ± 3	30 ± 4	232 ± 12	1.6
7	4.9 ± 1.1	2343 ± 283	43 ± 2	–	5 ± 1	3	294 ± 15	2.1
8	8.6 ± 1.3	2982 ± 324	57 ± 2	57 ± 2	28 ± 3	26 ± 2	265 ± 11	2.4
9	44.1 ± 2.5	2875 ± 315	61 ± 3	55 ± 4	142 ± 18	147 ± 17	58 ± 2	–
10	50.0 ± 3.2	2809 ± 398	63 ± 3	59 ± 5	150 ± 5	160 ± 6	57 ± 3	–
11	31.2 ± 1.2	2747 ± 120	61 ± 3	61 ± 3	171 ± 13	178 ± 15	40 ± 2	–
12	10.4 ± 1.7	2933 ± 165	57 ± 2	57 ± 2	137 ± 20	119 ± 13	177 ± 12	–
13	54.9 ± 6.6	3037 ± 352	63 ± 6	57 ± 4	147 ± 14	154 ± 17	59 ± 2	–
14	9.2 ± 0.6	2459 ± 292	56 ± 6	56 ± 6	12 ± 1	10 ± 1	799 ± 43	2.3
15	4.3 ± 1.1	3318 ± 205	53 ± 1	–	4 ± 1	3	285 ± 17	2.2
PA	4.8 ± 0.7	2541 ± 193	71 ± 3	71 ± 3	84 ± 13	85 ± 12	–	–
NC	–	–	–	–	–	–	–	4.8

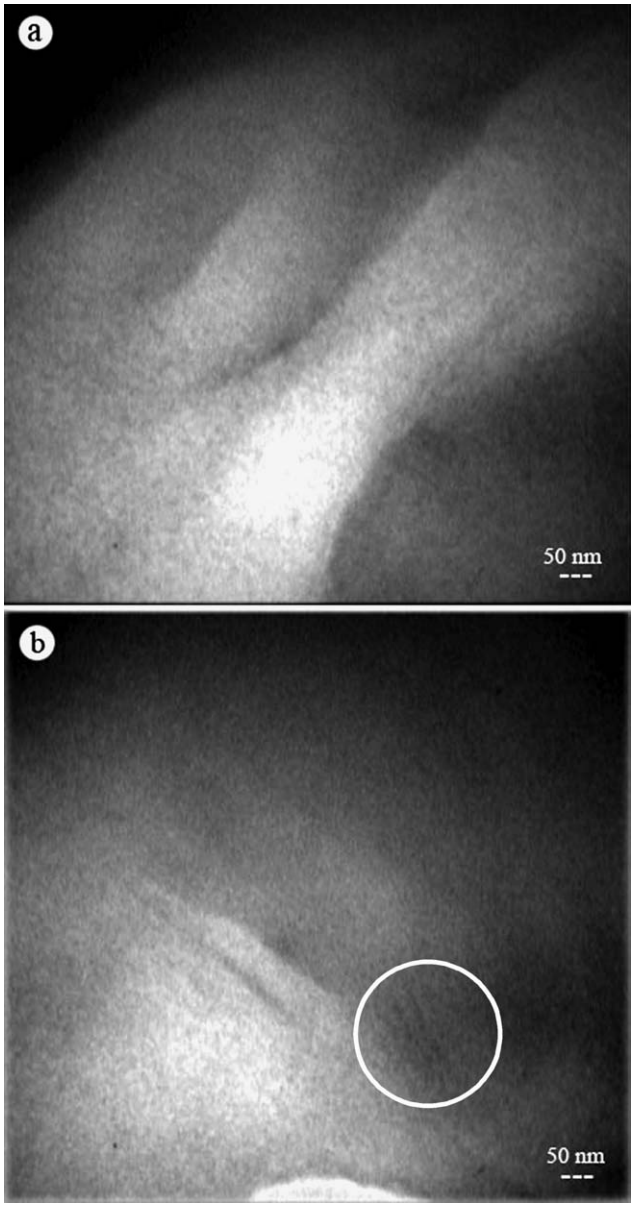

Figure 2 TEM micrograph of (a) sample No. 2 and (b) sample No. 5.

darker or lighter zones in the phase images, too. Therefore, the dark streaks (areas) in the phase images may be misinterpreted as a different phase, while they are appeared only as a result of variation in the height of the surface. The problem would be more labyrinthine when both phase and height change simultaneously.

The phase and the height images of sample No. 2 are shown in Figure 3. The dark streaks in Figure 3(b) are showing the dispersed nanoclay in polyamide 6 matrix. The thicker streaks would be an indication of nonexfoliated clay particles. Notice that nanoclay particles rotation in the polyamide 6 matrix should be taken into account. Although the exfoliated structure is achieved, rotation of the clay platelets may result in appearing thicker streaks in phase images. However, three different tests (TEM, XRD, and AFM) confirm the well exfoliated nanostructure. Figure 3(c,d) is showing the dispersion of the rubber particles throughout the compound. The absence of the clay clusters in the phase image demonstrates well exfoliation of the clay platelets.

The topography and phase images of the sample No. 5 is shown in Figure 4. These images are covering an area with the surface of 500×500 cm^2. The dark lines locating around the white circles would be an indication of placing the clay particles in rubber-matrix interfacial region. It would be worthwhile to mention that the thickness of these streaks could be due to intercalated (nonexfoliated) nanostructure as well as rotation of the clay particles.

Response function

The results obtained from the tensile and the notched Izod impact tests are summarized in Table II. By linear regression analysis of eq. (2) for notched Izod impact strength of the compounds, the numerical values for coefficients were obtained. A total of 15 experiments, including three levels of every parameter, allow fitting a cubic response surface model as a function of rubber type, clay content, and rubber content:

$$\eta = \beta_0 + \beta_1 x_1 + \beta_2 x_2 + \beta_3 x_3 + \beta_{11} x_1^2 + \beta_{22} x_2^2 + \beta_{33} x_3^2 + \beta_{12} x_1 x_2 + \beta_{13} x_1 x_3 + \beta_{23} x_2 x_3 \quad (3)$$

Response surfaces of the impact resistance fitted to data are summarized in Table III. The *R*-square value, roughly around 82%, illustrates that the model is able to explain 82% of the variability in the impact resistance over variables domain. Furthermore, the *P*-values (the pure quadratic coefficient estimate or a measure of the statistical significance) of clay content term, suggest this parameter sounds to be the most significant parameter. A procedure for evaluation of the adequacy of the fitted model is called testing *lack of fit* of the fitted model. The *P*-value for lack of fit is 0.048 suggesting that this model acceptably fits the data.

Main effects plot

Main effects plot is employed to plot average values when there are multiple factors. The points in the plot are the average of the response variable at the various levels of every factor, with a reference line drawn at the grand mean of the response data. The main effects plot is usually used to compare importance of main effects. The main effects plot for 15 series of the experiments is shown in Figure 5. Figure

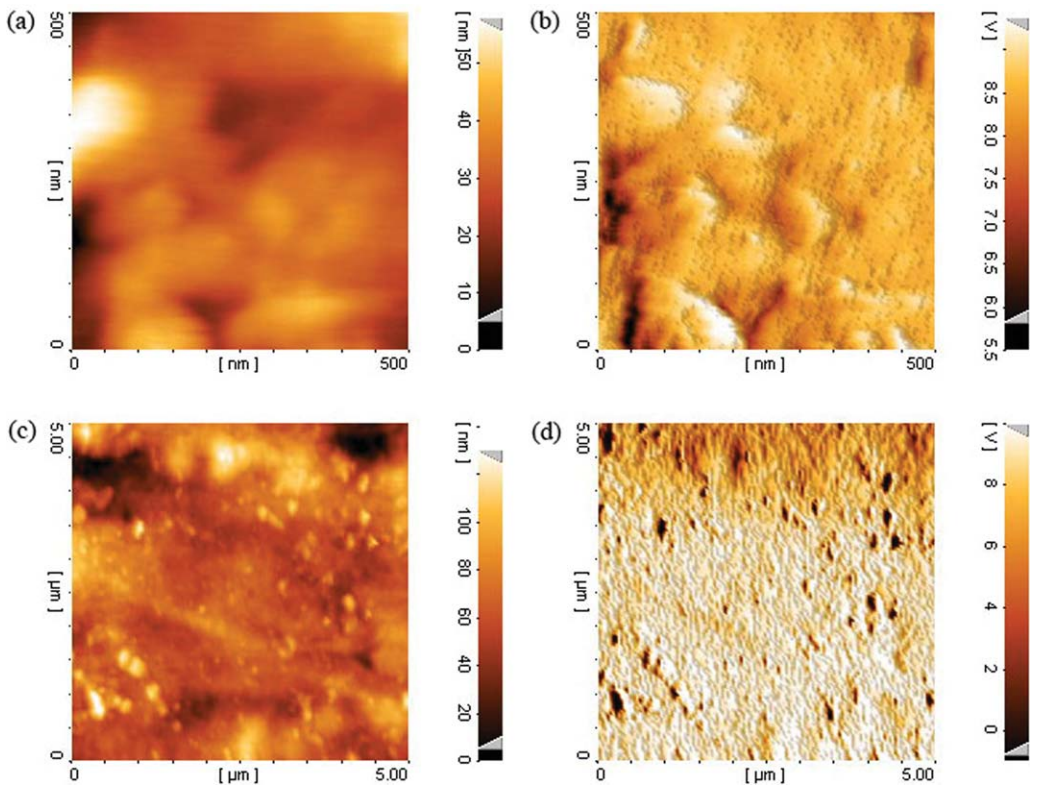

Figure 3 AFM topography (left) and phase (right) images of sample No. 2. The fields of view are 500×500 nm [(a) and (b)] and 5 × 5 µm [(c) and (d)]. [Color figure can be viewed in the online issue, which is available at www.interscience.wiley.com.]

5(a) indicates among Lotryl 29MA03, Lotader 4700 and HNBR, Lotader would be the best option to attain a high impact resistance compound. The high impact strength is attributed to ultrafine rubber particles in polyamide matrix. Figure 6 shows the phase morphology of the samples Nos. 13 and 2, respectively. The interfacial reaction between amide end groups of polyamide 6 and maleic anhydride groups of E-EA-MAH reduces the interfacial tension and enhances the adhesion between phases, finally leading to lower values of matrix ligament thickness in nanocomposites blends. Larger rubber particles in the compounds containing E-MA and HNBR (Fig. 7) because of higher interfacial tension of polyamide 6 matrix and toughers leading to larger ligament thickness is one of the possible causes for lower impact strength of these compounds. The mean particle size of the rubber particles are shown in Table II.

Figure 5(b,c) shows general trend of impact resistance of the compounds versus rubber and clay content which decreases with increasing clay loading and with decreasing rubber content, as expected. Correlations between rubber concentration and toughness have been reported for many rubber-

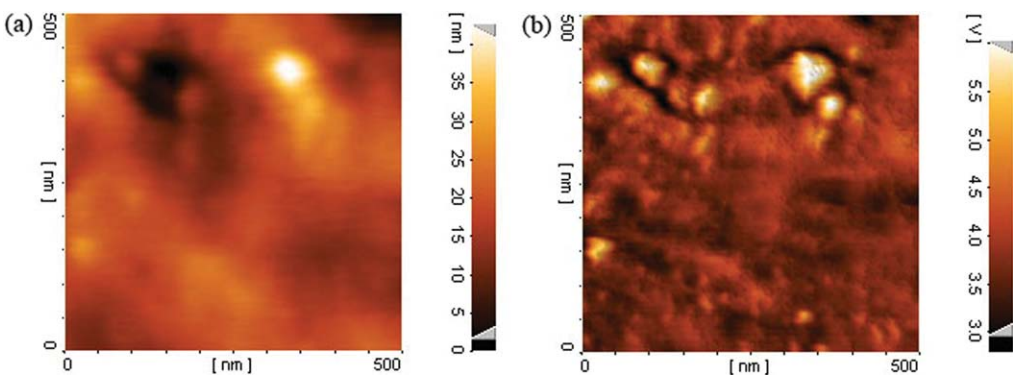

Figure 4 AFM topography (left) and phase (right) images of sample No. 5. The field of view is 500 × 500 nm. [Color figure can be viewed in the online issue, which is available at www.interscience.wiley.com.]

TABLE III
Parameter Estimates and the Statistical Results of Full Quadratic Response Surface Approximation for Impact Resistance of Polyamide 6 Based Hybrid Nanocomposites

Term	Estimate	*P*
Constant(β_0)	49.6933	0.006
Rubber type(β_1)	−1.1900	0.866
Clay content(β_2)	−13.7788	0.096
Rubber content(β_3)	7.9088	0.292
Rubber type*rubber type(β_{11})	−36.8304	0.014
Clay content*clay content(β_{22})	−5.0129	0.634
Rubber content*rubber type(β_{33})	−5.1279	0.626
Rubber type*clay content(β_{12})	−0.4750	0.962
Rubber type*rubber content(β_{13})	−0.5500	0.956
Clay content*rubber content(β_{23})	−17.1025	0.132

The lower *P*-values demonstrate that the term is more significant.

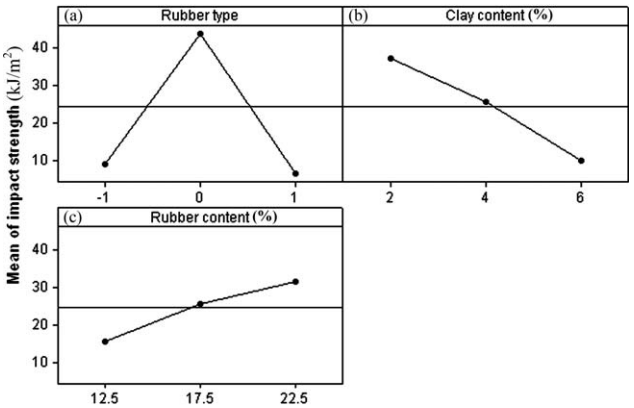

Figure 5 Main effects plot (data means) for notched Izod impact strength of the prepared compounds. The rubber types, −1, 0, and 1 stand for HNBR, Lotader 4700 and Lotryl 29MA03, respectively.

modified polymers.[30–32] A complication in correlating concentration of rubber particles to fracture behavior arises from microstructural features, such as particle size, particle size distribution, and internal particle structure that are all often interrelated, so it is difficult to progressively change one feature independently of the others. Generally, the impact strength of the rubber filled compounds passes through a maximum at about 20 wt %.[33] This maximum occurs because at higher concentration the rubber phase does not form a separate particulate phase, but a single-phase or combination of a matrix-disperse and co-continuous blend (intermediate morphology) is produced. Although run Nos. 5 and 7 involving 22.5 wt % of Lotader and Lotryl show intermediate morphology (Fig. 8), the impact resistance of the compounds, in general, increases when the rubber content varies from 17.5 to 22.5 wt % of rubber. As mentioned earlier, the main effects plot is used to plot data means, therefore the impact resistance of the compounds at each level of rubber and clay content, would be an average of all compounds containing a certain amount of clay or rubber.

Inactivating dissipating energy mechanisms, formation of intermediate morphology (combination of co-continuous and matrix-disperse) reduces the impact strength of both reactive and nonreactive blends significantly. The Izod impact strength of samples Nos. 5 and 7 are 13.7 and 4.9 kJ/m^2, respectively.

Willemse et al.[34] denoted that for the minor phase to become continuous within the major phase, certain requirements for its shape should be fulfilled. In particular, at low volume fraction of rubber, co-continuity can only be present if the minor blend components consist of structures with an expanded shape. Only then this component is capable of forming a continuous network. Figure 9 shows that sample No. 15 has elongated morphology and might be entering into the co-continuity region. In addition, this sample contains 6 wt % of nanoclay (the highest content) preventing the energy dissipating during impact test. Furthermore, it should be noted that there is maximum clay content beyond which toughening does not occur. It is credible that the high clay concentration system makes the nanocomposite behave as micrometer sized filler filled system.[35] However, the X-ray diffraction demonstrates the exfoliation/intercalation morphology in all samples. The representative stress–strain curves of samples

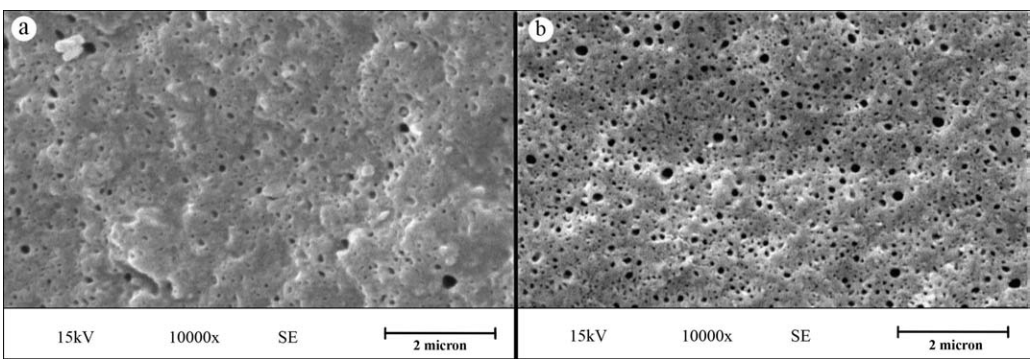

Figure 6 SEM micrographs of cross-sectional area of (a) sample No. 13 (b) sample No. 2 at 10,000× magnification.

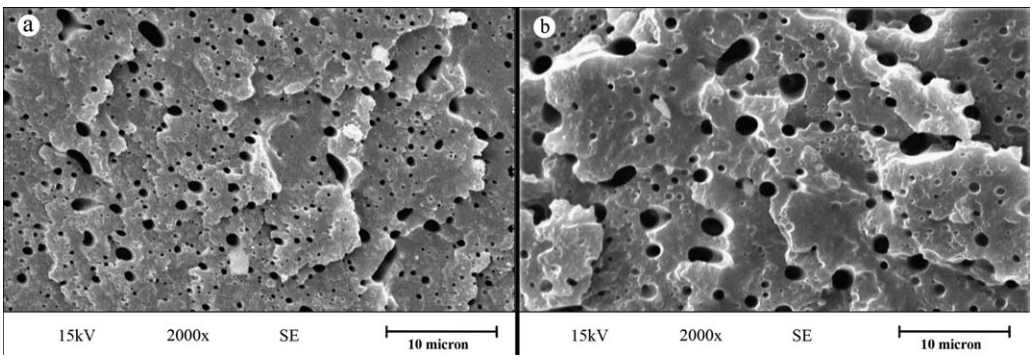

Figure 7 SEM micrographs of cross-sectional area of (a) sample No. 4 (b) sample No. 14 at 2000× magnification.

Nos. 5, 7, and 15 are shown in Figure 10. These curves confirm the intermediate morphology formation preventing energy dissipation during impact test. As can be seen, no yielding occurs under a low speed tensile test, indicating no yielding will also occur while crack propagation under a high speed impact test (Izod impact test).

Interactions plot

An interactions plot is a plot of averages for every level of a factor with the level of a second factor held constant. Interactions plots are valuable for evaluating the presence of the interaction. Interaction exists when the response at a factor level depends upon the level(s) of other factors. Parallel lines in an interactions plot reveal no interaction between parameters. The greater the departure of the lines from the parallel state, the higher the degree of interaction. An interaction between factors takes place when the change in response from the low level to the high level of one factor is not the same as the change in response at the same two levels of a second factor. That is, the effect of one factor depends on a second factor. Interactions plots can be brought into play to compare the relative strength of the effects across factors. The interactions plot for 15 series of experiments in this study has been shown in Figure 11. This figure provides very useful information about systems studied in this work including different types of toughenes. Figure 11(a) indicates that the interaction between clay content and rubber type is much greater when using Lotader, i.e., the change in the impact strength of the samples from the low level to the high level of clay content is approximately the same for both Lotryl and HNBR but varies for the Lotader considerably. In other words, increase in the clay content affects slightly the impact strength of the compounds involving Lotryl and HNBR but significant effect is observed on the impact strength of the compounds including Lotader. Figure 11(b) reveals almost the similar trend for impact strength versus rubber content using Lotryl and HNBR. Although improvement in the impact strength of compounds with increasing the rubber content was expected, this trend was not observed for Lotryl and HNBR rubbers. The impact resistance of the compounds containing these types of rubbers was almost unchanged while increasing the amount of rubber from 12.5 to 22.5 wt %. Nevertheless, increase in the content of Lotader 4700 (interactive rubber) enhanced the impact strength of the compounds considerably. Figure 11(c) shows a high degree of interaction between clay content and rubber content. This figure reveals that impact strength shows an optimum (minimum or maximum) when the rubber content changes from the low level to the high level in different levels of clay

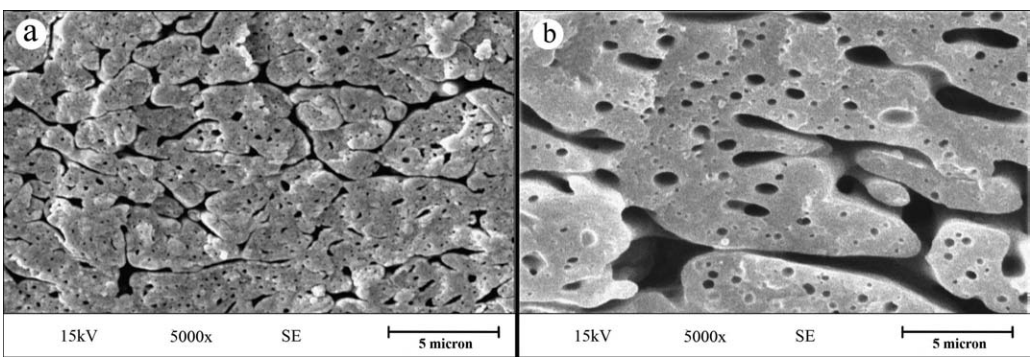

Figure 8 SEM micrographs of cross-sectional area of (a) sample No. 5 (b) sample No. 7 at 5000× magnification.

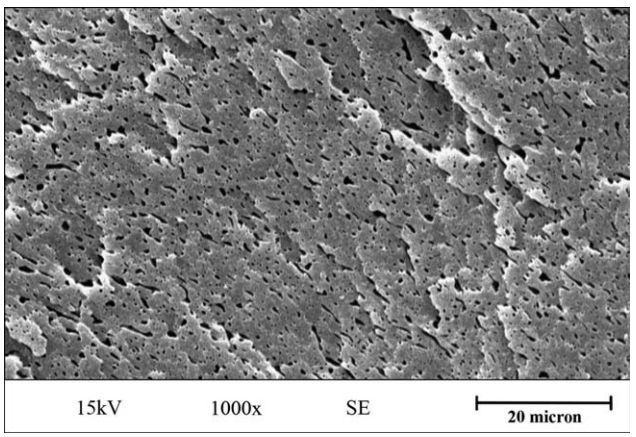

Figure 9 SEM micrographs of cross-sectional area of sample No. 15 at 1000× magnification.

content. At 2 and 6 wt % of nanoclay, the impact strength of compounds passes through a minimum, opposite to compounds containing 4 wt % of clay content. Depression of the impact strength with increasing of rubber content from 12.5 to 17.5 wt %, at constant clay content of 2 wt % is attributed to the spirit of interactions plot. The value of impact strength at 17.5% of rubber is, indeed, the average of impact strength of all samples containing 2% of organoclay and 17.5% of rubber content, i.e., this value is the average of the impact strength of run Nos. 12 and 14 which contain rubber types of −1 (HNBR) and 1 (Lotryl), respectively. Therefore, the lower impact strength of compounds containing 17.5% of rubber compared with compounds including 12.5% of rubber verifies because of lower impact resistance of nanocomposites containing −1 (HNBR) and 1 (Lotryl) rubbers.

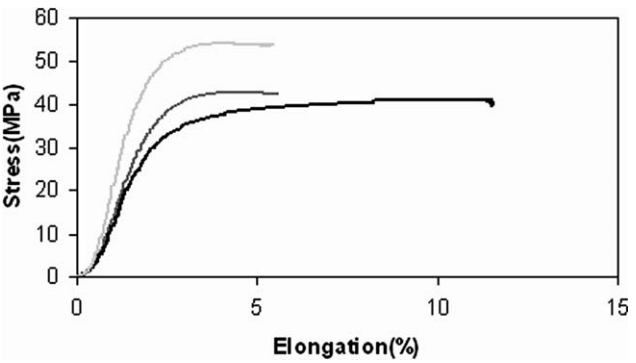

Figure 10 Tensile stress vs. strain curves of samples No. 5, 7, and 15. Black, gray, and light gray curves show tensile curves of samples No. 5, 7, and 15, respectively.

Contour plots

Contour plot is used to visualize the response surface. Contour plots are useful for setting up desirable response values and operating conditions. A contour plot shows how a response variable relates to two factors based on a model equation. As a contour plot shows only two factors at a time, any extra factor are kept at a constant level. Consequently, the contour plots are merely valid for fixed levels of the extra factors. If the holding levels change, the response surface changes as well, sometimes significantly. In this article, the factors held at their middle points for plotting the contours. Figure 12 shows the contour plots of impact resistance of the compounds. This plot shows how clay content and rubber type, rubber content and rubber type, rubber content and clay content are related to impact resistance when the third factor is at its middle level. The darker area indicates the contour where the response is higher. Figure 12(a) shows contour plots of the

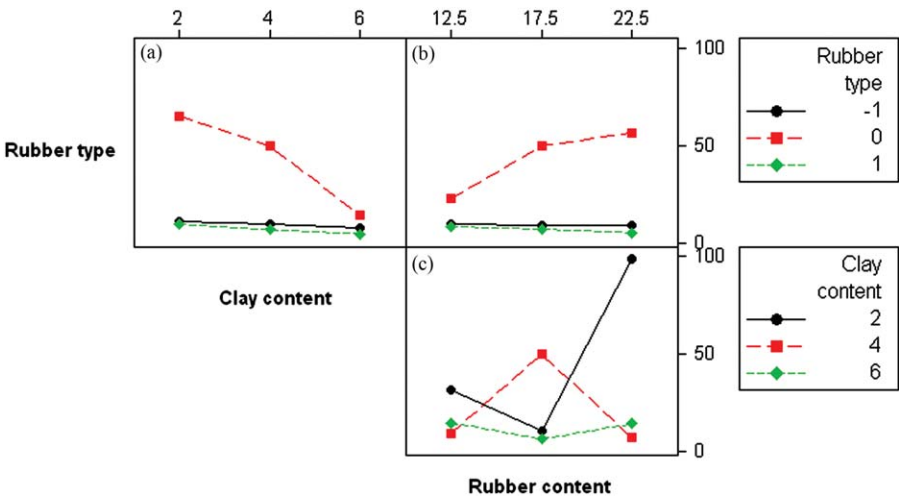

Figure 11 Interaction plot (data means) for notched Izod impact strength of the prepared compounds. The rubber types, −1, 0, and 1 stand for HNBR, Lotader 4700 and Lotryl 29MA03, respectively. [Color figure can be viewed in the online issue, which is available at www.interscience.wiley.com.]

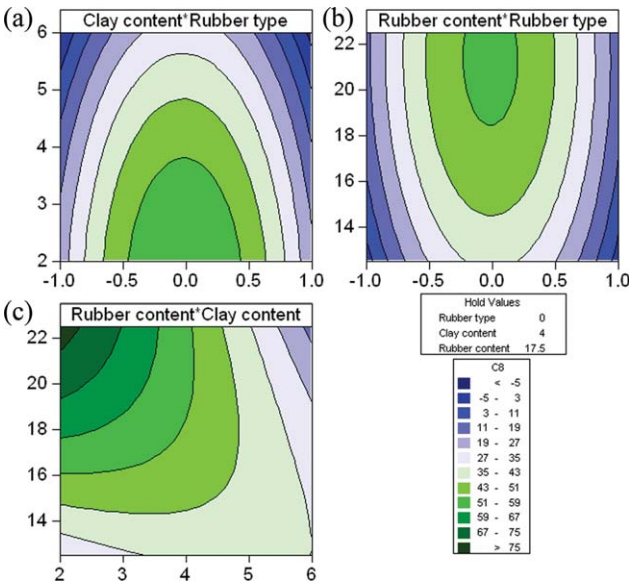

Figure 12 Contour Plots of notched Izod impact strength of the prepared compounds. The rubber types, −1, 0, and 1 stand for HNBR, Lotader 4700 and Lotryl 29MA03, respectively. [Color figure can be viewed in the online issue, which is available at www.interscience.wiley.com.]

impact strength as a function of rubber type and clay content at a rubber content of 17.5 wt %. The response surface indicates that compounds with the impact resistance ranging from 51 to 59 kJ/m^2 can be obtained over a range of clay content, roughly around 3–4.7 wt %, and lower level of clay content yields compounds with higher impact resistance. Also, this figure shows that the impact strength decreases as the clay content is increased when using any kinds of rubbers, as expected. Figure 12(b) showing the contour plots of the mean impact strength provides information on the correlation between the rubber content and rubber type at constant level of clay content (4 wt %). This figure shows that to achieve compounds with the impact resistance ranging from 51 to 59 kJ/m^2 at least 19 wt % of Type 0 rubber (Lotader 4700) is required. In addition, this figure reveals that other types of rubbers (nonreactive rubbers) are not effective enough to improve the impact resistance of polyamide 6 based compounds as well as reactive rubber while using 4% of montmorillonite.

Figure 12(c) indicates that to maximize the impact strength (around 20 times improvements in impact strength of the compound compared with pristine polyamide 6 resin) while using rubber Type 0 (E-EA-MAH), clay and rubber content should be chosen at their lowest and highest level, respectively. It demonstrates that there is a specific region for achieving the compounds with the highest impact resistance.

Condition for optimum response

In semicrystalline polymers, important toughening is obtained with dispersion of rubber particles. However, adding rubber most often persuades a significant loss in elastic modulus. In this study, we investigate how to avoid such softening by simultaneous application of rubber phase and nanoclay. Response optimization is used to help recognizing the combination of input parameters settings that jointly optimize a single response or a set of responses. It is possible to evaluate the importance of each response to assign appropriate values for response. For calculation of optimum design, the importance of impact strength was chosen twice than Young's modulus.

Figure 13 shows the optimization plot for this condition. Each row, indeed, represents the main effect plots for each response. This figure shows that every factor affects the Young's modulus and impact resistance differently, implying difficulties regarding optimization process. The numbers displayed at the top of a column show the current factor level settings (red-colored row) and the high and low factor settings in the experimental design. For example, the current factor settings are rubber type = 0(E-EA-MAH), clay content = 3.7716, and rubber content = 17.0888. The composite desirability (D) which combines the individual desirability of all the response variables into a single measure is displayed in the upper left corner of the graph. According to calculations, choosing 0 (E-EA-MAH), 3.7716 and 17.0888 for rubber type, clay content and rubber content, respectively, yields the 2896.7792, 50.3556, and 0.56161 values for Young's modulus, impact resistance, and composite desirability, correspondingly. This optimum condition is exceedingly close to the design points with all factor levels set halfway between the low and high settings.

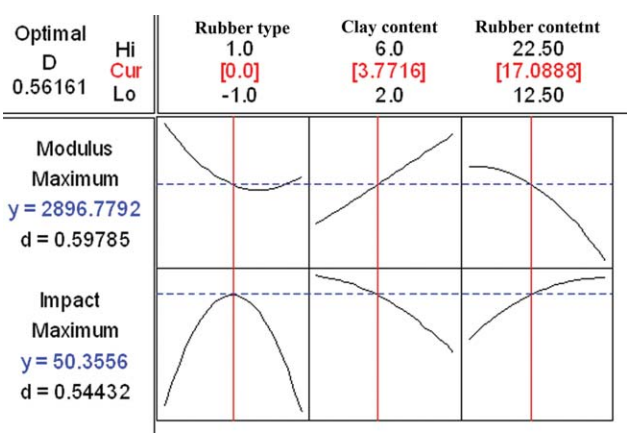

Figure 13 Optimization plot for Izod notched impact strength and Young's modulus of the prepared compounds. The red-colored row implies the optimum condition. [Color figure can be viewed in the online issue, which is available at www.interscience.wiley.com.]

CONCLUSIONS

An experimental investigation of material parameters to produce toughened polyamide 6 nanocomposites was carried out. The goal was to investigate the interactive and main effects of the parameters on the resultant impact strength and to establish a prediction scheme for the domain/window of the parameters where targeted impact strength can be achieved. The planning of the experiments and the analysis of the results were performed within the context of response surface methodology featuring design of experiments and linear regression analysis. Sets of experiments were performed at three different types of rubbers and three different levels of organoclay and rubbers. The analysis of the experiments suggest the following conclusions in toughening of polyamide 6/rubber/clay system studied here:

- Using ethylene-ethyl acrylate-maleic anhydride as toughener, 4 wt % of clay and 17.5 wt % of the toughener, the best balanced mechanical properties were achieved, whereas impact strength and Young's modulus were improved 900% and 15%, respectively. On the other hand, the sample containing ethylene-ethyl acrylate-maleic anhydride as toughener, 2 wt % of clay and 22.5 wt % of the toughener showed the best impact resistance, whereas notched Izod impact strength improved 2050% and Young's modulus depressed only 15%.
- Clay content was found to be a significant factor to determine the impact resistance of the compound.
- The impact strength of the hybrid nanocomposites increases with increasing of rubber content before reaching phase inversion point.
- Inactivating dissipating energy mechanisms, formation of intermediate morphology (combination of co-continuous and matrix-disperse) reduce the impact strength of both reactive and non-reactive blends significantly.
- The interactive effects of the investigated parameters were demonstrated using interaction plot.
- A rough estimation of the morphology of the produced compounds should be taken into account for designing a formulation outside of the investigated range.

The authors would like to thank Arkema Chemicals for providing some of our required materials.

References

1. Isik, I.; Yilmazerand, U.; Bayram, G. Polym Compos 2007, 29, 133.
2. González, I.; Eguiazábal, J. I.; Nazábal, J. Eur Polym J 2006, 42, 2905.
3. Wang, K.; Chen, L.; Wu, J.; Toh, M. L.; Heand, C.; Yee, A. F. Macromolecules 2005, 38, 788.
4. Dasari, A.; Yu, Z.-Z.; Yang, M.; Zhang, Q.-X.; Xieand, X.-L.; Mai, Y.-W. Compos Sci Technol 2006, 66, 3097.
5. Gonzalez, I.; Eguiazabaland, J. I.; Nazabal, J. Compos Sci Technol 2006, 66, 1833.
6. Dong, W.; Zhang, X.; Liu, Y.; Gui, H.; Wang, Q.; Gao, J.; Song, Z.; Lai, J.; Huangand, F.; Qiang, J. Eur Polym J 2006, 42, 2515.
7. Liu, X.; Wu, Q.; Berglund, L. A.; Lindberg, H.; Fanand, J.; Qi, Z. J Appl Polym Sci 2003, 88, 953.
8. Shishan, W.; Dingjun, J.; Xiaodong, O.; Fenand, W.; Jiang, S. Polym Eng Sci 2004, 44, 2070.
9. Jiang, T.; Wang, Y.; Yehand, J.; Fan, Z. Eur Polym J 2005, 41, 459.
10. Dong, W.; Liu, Y.; Zhang, X.; Gao, J.; Huang, F.; Song, Z.; Tanand, B.; Qiao, J. Macromolecules 2005, 38, 4551.
11. Vlasveld, D. P. N.; Groenewold, J.; Berseeand, H. E. N.; Picken, S. J. Polymer 2005, 46, 12567.
12. Chang, J.-H.; Park, K. M.; Cho, D.; Yangand, H. S.; Ihn, K. J. Polym Eng Sci 2001, 41, 1514.
13. Yano, K.; Usuki, A.; Kurachiand, T.; Kamigaito, O. J polym Sci Part A: Polym Chem 1993, 31, 2493.
14. Kelnar, I.; Stephan, M.; Jakischand, L.; Fortenlý, I. J Appl Polym Sci 2000, 78, 1597.
15. Muratoglu, O. K.; Argonand, A. S.; Cohen, R. E. Polymer 1995, 36, 921.
16. Kayano, Y.; Keskkulaand, H.; Paul, D. R. Polymer 1998, 39, 2835.
17. Burgisi, G.; Paternoster, M.; Pedutoand, N.; Saraceno, A. J Appl Polym Sci 1997, 66, 777.
18. Choand, J. W.; Paul, D. R. Polymer 2001, 42, 1083.
19. Kelnar, I.; Khunoná, V.; Kotekand, J.; Kaprálková, L. Polymer 2007, 48, 5332.
20. Dasari, A.; Yuand, Z.-Z.; Mai, Y.-W. Polymer 2005, 46, 5986.
21. Ahnand, Y.-C.; Paul, D. R. Polymer 2006, 47, 2830.
22. Yördem, O. S.; Papilaand, M.; Menceloğlu, Y. Z. Mater Des 2008, 29, 34.
23. Saeband, M. R.; Garmabi, H. J Appl Polym Sci 2009, 111, 1600.
24. Guand, S.-Y.; Ren, J. Macromol Mater Eng 2005, 290, 1097.
25. Sukigara, S.; Gandhi, M.; Ayutsede, J.; Micklusand, M.; Ko, F. Polymer 2004, 45, 3701.
26. Chen, Y.-D.; Pengand, J.; Lui, W.-B. J Appl Polym Sci 2009, 113, 258.
27. Luoand, J.-J.; Daniel, I. M. Comp Sci Tech 2003, 63, 1607.
28. Maitiand, M.; Bhowmick, A. K. J Polym Sci Part B: Polym Phys 2006, 44, 162.
29. Liuand, T. X.; Liu, Z. H. Comp Sci Tech 2003, 63, 331.
30. Pegorettiand, A.; Ricco, T. Eng Fract Mech 2006, 73, 2486.
31. Baldi, F.; Bignotti, F.; Tieghiand, G.; Riccò, T. J Appl Polym Sci 2006, 99, 3406.
32. Gonzalez, I.; Eguiazabaland, J. I.; Nazabal, J. J Polym Sci Part B: Polym Phys 2005, 43, 3611.
33. Kinlochand, A. J.; Young, R. J. Fracture Behaviour of Polymers; Elsevier Applied Science: London, New York, 1983.
34. Willemse, R. C.; De Bore, A. P.; Damand, J. V.; Gotsis, A. D. Polymer 1998, 39, 5879.
35. Sheng, N.; Boyce, M. C.; Parks, D. M.; Rutledge, G. C.; Abesand, J. I.; Cohen, R. E. Polymer 2004, 45, 487.